NUCL SCI TECH (2022) 33:95
https://doi.org/10.1007/s41365-022-01082-2

Nuclear design of an integrated small modular reactor based on the APR-1400 for RO desalination purposes

Reem Rashed Alnuaimi[1] · Bassam Khuwaileh[1] · Muhammad Zubair[1] · Donny Hartanto[2]

Received: 27 February 2022 / Revised: 29 June 2022 / Accepted: 1 July 2022 / Published online: 9 August 2022

Abstract The United Arab Emirates lacks conventional water resources and relies primarily on desalination plants powered by fossil fuels to produce fresh water. Nuclear desalination is a proven technology, cost-competitive, and sustainable option capable of integrating the existing large-scale desalination plants to produce both freshwater and electricity. However, Small Modular Reactors (SMRs) are promising designs with advanced simplified configurations and inherent safety features. In this study, an Integrated Desalination SMR that produces thermal energy compatible with the capacity of a fossil fuel-powered desalination plant in the UAE was designed. First, the APR-1400 reactor core was used to investigate two 150 MW_{th} conceptual SMR core designs, core A and core B, based on two-dimensional parameters, radius, and height. Then, the CASMO-4 lattice code was used to generate homogenized few-group constants for optimized fuel assembly loading patterns. Finally, to find the best core configuration, SIMULATE-3 was used to calculate the core key physics parameters such as power distribution, reactivity coefficients, and critical boron concentration. In addition, different reflector materials were investigated to compensate for the expected high leakage of the small-sized SMR cores. The pan shape core B model (142.6132 cm diameter, 100 cm height, and radially reflected by Stainless Steel) was selected as the best core configuration based on its calculated physics parameters. Core B met the design and safety criteria and indicated low total neutron leakage of 11.60% and flat power distribution with 1.50 power peaking factor. Compared to core A, it has a more negative MTC value of −6.93 pcm/°F with lower CBC. In a 2-batch scheme, the fuel is discharged at 42.25 GWd/MTU burnup after a long cycle length of 1.58 years. The core B model offers the highest specific power of 36.56 kW/kgU while utilizing the smallest heavy metal mass compared with the SMART and NuScale models.

Keywords Nuclear desalination · Small modular reactor (SMR) · APR-1400 · CASMO-4 · SIMULATE-3 · Two-step method · Homogenized cross sections · Optimization

1 Introduction

The United Arab Emirates is located in the dry belt region, distinguished by high temperatures and a scarcity of rain, with an annual precipitation average of about 100 mm, classifying it as an arid zone [1]. With the tremendous increase in population, water preserves a fundamental pillar of urbanization, as most of the groundwater in the country was used in agricultural, industrial, and economic activities. Thus, the demand increased while the conventional water resources were insufficient; this raised concerns about water security. Due to the strategic location of the UAE on the coastline of the Arabian Gulf, seawater desalination was a long-term option to provide the water needed to cover the demand. Indeed, water desalination technology was first used in Abu Dhabi in 1976 with a capacity of 66,000 gal/d. Today, more than 70 desalination plants are distributed along with the Emirates, providing

✉ Reem Rashed Alnuaimi
U17100889@sharjah.ac.ae

[1] Department of Mechanical and Nuclear Engineering, University of Sharjah, P.O. BOX 27272, Sharjah, UAE

[2] Oak Ridge National Laboratory, 1 Bethel Valley Road, Oak Ridge, TN 37830, USA

42% of the country's water requirements and representing 14% of the desalinated water worldwide [2].

Desalination is the process of separating nearly salt-free fresh water from a sea or brackish water, while salts are concentrated in a rejected brine stream. Historically, Aristotle (384–322 BC) described the possibility of desalinating water in his meteorology book. Furthermore, freshwater production tools have been designed since antiquity and the medieval ages; however, large-scale desalination plant development began in the 1930s [3]. The technologies used in desalination are varied, such as Multi-Stage Flash (MSF) and Multi-Effect Distillation (MED) and thermally driven processes, and Reverse Osmosis by employing membranes to produce freshwater [4].

The Multi-Stage Flash (MSF) is a procedure that involves increasing the pressure of incoming seawater and heating it to near-boiling temperatures. The seawater pressure is reduced in stages, resulting in a vapor that is condensed by the incoming seawater. The Multi-Effect Distillation (MED) process, on the other hand, uses a steam heat source and a series of evaporators at gradually lower pressures to produce freshwater [5]. From total dissolved solids (TDS) levels as high as 60,000–70,000 mg/L, thermal desalination processes can produce water with very low salinity levels of 10 mg/L or less. However, distillation processes for seawater desalination have limitations. For example, evaporation consumes between 25 and 100 kWh per 1000 gal of freshwater, limiting thermal desalination capability in countries with high energy costs. Furthermore, due to the highly corrosive nature of seawater, thermal desalination suffers from operational issues such as corrosion and scaling, which necessitates the use of special alloys in the plant material, raising the capital cost of the plant [6].

Membrane desalination was discovered as part of significant desalination research conducted in the 1960s in the United States [7]. It primarily operates by utilizing electricity to apply an external pressure source more significant than the osmotic pressure of seawater. It will force seawater through a semipermeable membrane that selectively allows water to pass through it faster than any components present in the water are transported [8]. As a result, it causes the freshwater to reverse into a less robust solution while the brine collects on the pressurized side, known as reverse osmosis (RO) [9]. The first commercial Seawater Reverse Osmosis (SWRO) plants were installed in Saudi Arabia in 1975, and there are currently more than 1000 SWRO plants constructed around the world. The commercially available SWRO membranes can reject 99.5–99.8% of the total dissolved solids (TDS) in the saline feedwater. In addition, because membrane processes are based on physical separation, they don't require thermal energy to vaporize the water. As a result, the energy consumption for the treatment of an SWRO plant typically ranges between 10 to 20 kWh per 1000 gal of freshwater [6]. Today, reverse osmosis accounts for almost 2/3 of the global desalination capacity, and it is recognized as the fastest developing desalination technology [7].

Besides, to meet the UAE's growing demand for desalinated water, which is expected to reach 8.8 billion cubic meters per year by 2030, efforts are being made to expand the capacity of existing desalination plants and construct new ones [2]. However, all desalination technologies share high energy requirements to generate the required heat and electricity via fossil fuel-powered stations. According to a 2018 statistic by the Global Clean Water Desalination Alliance, global emissions from worldwide desalination plants powered by fossil fuels amounted to around 76 million tons of CO_2 per year, and it is expected to reach about 218 million tons by 2040 [10]. Thus, the continuous reliance on desalination as an essential water source necessitates searching for alternative sustainable energy sources to power desalination plants without harming the environment. Therefore, the United Arab Emirates launched two remarkable strategies in 2017 as part of its visionary goals, "UAE Energy Strategy 2050" and "UAE Water Security Strategy 2036". The first aims to increase clean energy's contribution to the total energy mix from 25 to 50% while reducing power generation's carbon footprint by 70% [11]. On the other hand, the second aims to ensure sustainable access to water under all conditions. Furthermore, it addresses the use of advanced technologies, innovation, and the development of national capabilities in the field of water security [12].

Alongside hydropower, nuclear power is the backbone of Carbon-free power production, making nuclear desalination a prime candidate in the UAE. Nuclear desalination uses a nuclear reactor facility to generate the thermal and/or electrical power required for the desalination processes. The nuclear facility can be dedicated solely to the production of freshwater, or it can be used for freshwater and electricity co-generation, in which a portion of the reactor's total energy output is used for water production. In both cases, nuclear desalination is described as an integrated facility in which the reactor and the desalination system are on the same site, and energy is generated on-site for use in the desalination system [13]. The feasibility of connecting nuclear reactors to desalination plants has been investigated by the International Atomic Energy Agency (IAEA) since the 1960s [14]. Experience gained from using nuclear desalination plants, first in Japan with co-generation Ohi-I and Ohi-II PWR power plants utilizing the MSF process in 1973 [15], along with Kazakhstan BN-350 LMFR using the MED and MSF processes until 1999. However, by 2018, only 15 of the 15,906 operational desalination plants

in the world used nuclear energy, contributing less than 0.1% of desalination capacity [5].

In addition to the existing Gen-III large-scale reactors with capacities ranging from 1100 to 1600 MWe, the new design fleet of small modular reactors is gaining attention worldwide. Small Modular Reactors (SMRs) are small as their power rating is about 10–300 MWe, designed modularly with unit assembly Nuclear Steam Supply Systems in factories and assembled on-site [16]. SMRs are advantageous for countries starting nuclear programs or developing freshwater and electricity co-generation. Because of the shorter construction time, around three years, these types of reactors have a lower investment cost. Furthermore, nearly all of them have availability rates of at least 90% or higher, as well as inherent safety features that make them suitable for placement near population centers, lowering water transportation costs [5]. The SMR's small size and high level of modularity make combining a nuclear power plant with a desalination plant simple. The SMR's design, in particular, allows each module to use membrane and/or thermal desalination technologies. As a result, the integrated nuclear desalination plant's configuration can be set up to allow for maximum flexibility in selecting a desalination technology while also considering the plant's specific requirements [17].

Almost all nuclear power industry companies proposed SMR designs based on the structural features of their existing large-scale nuclear reactors, and 12 countries are pursuing the development of these reactors. The integral SMR type, in which the primary loop components, such as the steam generator and pressurizer, are integrated into the reactor pressure vessel and containment vessel, is increasingly recognized by nuclear reactor developers. The major attribute that distinguishes such a design from large-scale PWR is the coolant system, which increases safety margins by eliminating or decreasing some potential accident factors [17]. There are also several SMR designs in development based on gas-cooled reactors, such as the gas turbine-modular helium reactor (GT-MHR) and the pebble bed modular reactor (PBMR) [5]. Furthermore, preliminary neutronic assessments of new fuel cycle options, including thorium [18] and HALEU-based designs [19], are being investigated for a long-term improvement of the economic efficiency of SMRs. The IAEA anticipates that 96 SMRs will be operational by 2030 [20]. A significant milestone in SMR technology was achieved in Akademik Lomonosov in Russia with their floating power unit combining two module KLT-40 s connected to the grid and started operation in May 2020. In addition, two demonstration SMRs are nearing completion: the CAREM integral PWR in Argentina and the HTR-PM in China, both of which are expected to be operational within the next three years [21].

Research and development studies have also increased in many countries and are conducted under the IAEA umbrella or individual regulatory assistance to establish nuclear desalination infrastructure [13]. For example, in 2019, Saudi Arabia, having the highest desalination capacity globally, signed an official collaborative agreement with South Korea to construct the first nuclear-powered desalination plant using the SMART small modular reactor design. Moreover, China plans to utilize two small reactor concepts, the high-temperature-reactor-PM (HTR-PM) and the nuclear heat reactor (NHR), both prototypes of 200 MWe that can be used in nuclear desalination. Furthermore, Russia has two approaches for nuclear desalination: investing in the experience gained from the Atkau nuclear desalination plant in the form of a VVER 300 MW_{th} reactor coupled to a MED desalination process with a capacity of up to 170,000 m^3/d of freshwater or desalinating using a nuclear floating power unit comprised of two KLT-40 s small modular reactors [5].

Similarly, this study proposes a new SMR core design to increase installed desalination capacity and introduce nuclear desalination in the UAE. This study describes the first steps and sole UAE nuclear designing efforts in the scientific aspect of achieving water security goals through clean energy sources, enabling meeting its proactive strategies by the encouragement obtained through the UAE's latest operational milestones in the nuclear sector. It aims to keep up with the global renewed interest in the small modular reactor fleet and support the nation's desalination needs while emerging experience and drawing inspiration from the APR-1400 reactor design, currently used in four units at the UAE's Barakah Nuclear Power Plant.

In this study, an integrated desalination SMR is designed. The design objectives are:

1. Provide power comparable to that demanded by a reference Reverse Osmosis (RO) desalination plant (the Ghalilah desalination plant, United Arab Emirates).
2. Design an SMR core based on the APR-1400 concept.

First, the conceptual small modular reactor core design based on the APR-1400 reactor core was investigated. Then, the CASMO-4 lattice code was used to generate the homogenized few-group constants for fuel assemblies having different geometry and enrichments. Finally, the core key physics parameters such as the power distribution, reactivity coefficients, and critical boron concentration were calculated using SIMULATE-3.

2 Methodology

Designing a nuclear reactor requires predictions about how the neutrons will be distributed in the reactor core, determining how nuclear reactions will occur, and enabling us to infer the stability of chain reactions. Once the appropriate core's size and composition are chosen, the effective multiplication factor and neutron flux distribution are the most fundamental evaluation quantities in nuclear design calculations. Furthermore, they serve as the foundation for evaluating the core behavior discretized by reactivity coefficients and power distribution. This study's small modular reactor core design is intended to produce thermal power equivalent to the capacity of a fossil fuel-powered desalination plant in the UAE. The flow chart in Fig. 1 depicts the approach taken to investigate the conceptual SMR core design to find the optimum core configuration.

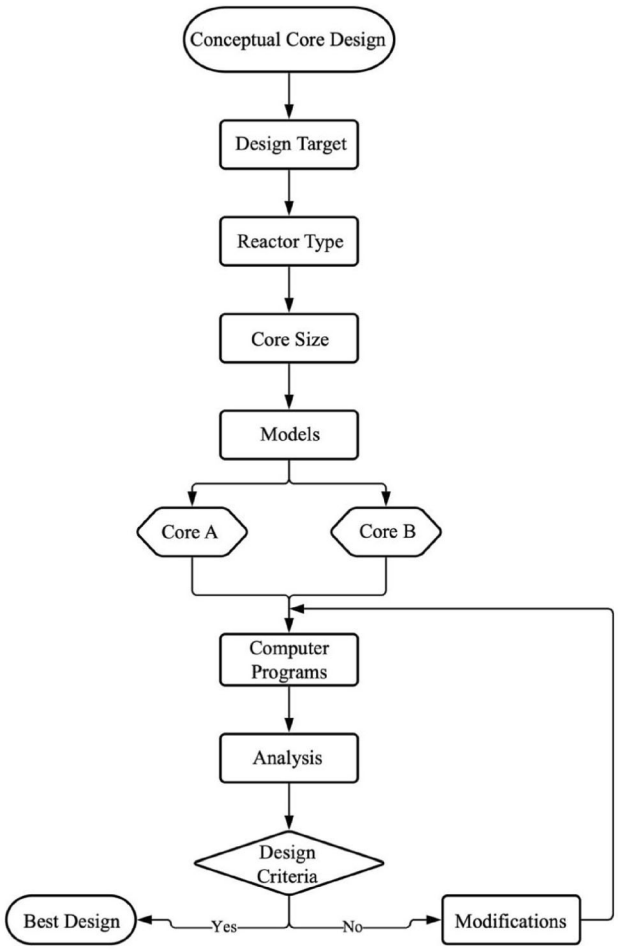

Fig. 1 Conceptual core design approach

2.1 Design target

Several desalination plants in the UAE were surveyed. The desalination plant at Ghalilah in the Emirate of Ras Al Khaimah, constructed by the Federal Electricity and Water Authority (FEWA) in partnership with Aquatech International, has been chosen for this SMR design model. Ghalilah plant provides vital freshwater to the distribution network of FEWA by producing 15 MIGD (68,000 m^3/d) of freshwater using Seawater Reverse Osmosis (SWRO) technology to treat seawater with salinity levels as high as 42,000 ppm from the Arabian gulf at 22 °C. The product is freshwater with salinity levels less than 500 ppm; detailed design water analysis is in Tables 1 and 2 [22]. This desalination plant will support the UAE Water Security Strategy 2036 Water Supply Management Program, which aims to provide future water needs more suitably by increasing the use of membrane desalination technologies [12]. In addition, since there is no thermal coupling between the reactor and the desalination plant, there is no direct path for the carryover of radioactive materials from the reactor to the product water.

The Ghalilah plant's overall energy consumption is 3.14 kWh/m^3 of freshwater due to the latest desalination technologies [23] which equals electricity consumption of 9 MW_e for reverse osmosis technology. Assuming the SMR has efficiency of 30%, the SMR core should produce about 30 MW_{th}. In this study, the SMR conceptual design is determined with overall thermal power of 150 MW_{th}, allowing it to be used for two options: 1) desalination only to meet the electricity needs of five facilities, such as the

Table 1 Ghalilah desalination plant inlet parameters [22]

Inlet Parameters	
pH	8.46
Turbidity (NTU)	30–35
TDS (ppm)	42,000
Calcium (ppm)	470
Magnesium (ppm)	1500
Sodium (ppm)	12,500
Potassium (ppm)	390
Bicarbonate (ppm)	98.57
Carbonates (ppm)	29.96
Chloride (ppm)	22,277
Sulfate (ppm)	3100
Boron (ppm)	4.1
Total hardness (ppm)	7,350
Temperature (°C)	18–36
Design temperature (°C)	22

Table 2 Ghalilah desalination plant outlet parameters [22]

Outlet Parameters	
pH	7.5–8.5
TDS (ppm)	≤ 500
Boron (ppm)	≤ 2.0
Chlorides (ppm)	≤ 200.0

Ghalilah plant (5 × 30 MW_{th} = 150 MW_{th}), and 2) co-generation of desalinated water and grid electricity supply, where (1 to 4) facilities like Ghalilah can be operated, and the remaining portion is used for other purposes.

2.2 Reactor type

Most SMRs are designed based on the structural features of a reference large-scale nuclear reactor. This SMR is selected to utilize the APR-1400 pressurized water reactor (PWR) design by Korea electric power corporation (KEPCO). The typical fuel assembly configurations of APR-1400, with a 16 × 16 array, contains 236 fuel rod positions, four guide thimbles, and one instrument tube, was used [24]. Fuel assembly design parameters are listed in Table 3. However, the fuel enrichment and burnable poison content in this SMR design were modified according to the fuel assembly's optimization results.

Table 3 Main design parameters [24]

Parameter	Value
Reactor thermal power (MW_{th})	150
Fuel temperature (K)	900
Moderator temperature (K)	580.4
Operating pressure (bar)	155
Boron concentration (ppm)	600
Lattice type	16 × 16
Number of fuel rods	236
Number of guide thimbles	4
Number of instrumentation tubes	1
Assembly pitch (cm)	20.60416
Fuel pin pitch (cm)	1.28776
Fuel pellet radius (cm)	0.409575
Fuel material	UO_2
Fuel pellet density (g/cm^3)	10.313
Fuel enrichment U-235 (%wt)	< 5%
Clad inner radius (cm)	0.41873
Clad outer radius (cm)	0.47600
Clad material	Zircaloy-2
Top reflector thickness (cm)	50
Bottom reflector thickness (cm)	50
Radial reflector thickness (cm)	15

2.3 Core size

The core dimensions can be modified depending on the thermal power output; to illustrate, this conceptual core design produces only 26.67% of the thermal power of the APR-1400. In this case, the APR-1400's 241 fuel assemblies must be reduced. Therefore, this SMR core size was reduced for efficient fuel use while conserving a similar linear power near APR 1400 value, approximately 18.380 kW/m [24]. To accomplish this, two-dimension parameters, the radius, and the height, were changed.

2.4 Models

As a result, two conceptual design models were proposed, core A and core B. Core A is a pencil shape with fewer fuel assemblies, whereas core B is a pan shape with more fuel assemblies, as shown in Fig. 2. Core configurations parameters are listed in Table 4.

2.5 Simulation methods

Nuclear reactor physics simulations are required to validate the proposed core A and B. A nuclear reactor's core contains several fuel assemblies, each containing a number of fuel elements of varying compositions, including separate fuel and cladding regions, structural components, and burnable poisons. Thus, a direct core calculation is challenging to perform in this heterogeneous geometry model using fine energy groups. Instead, the nuclear design calculation is performed in a two-step method: a lattice calculation in a two-dimensional (2D) infinite arrangement of fuel rods or assemblies and a core calculation in a three-dimensional (3D) whole core. The lattice calculation prepares few-group homogenized cross sections, which maintain the important energy dependence of nuclear reactions, reducing the core calculation cost in terms of time and memory. Both deterministic and Monte Carlo codes can be used in reactor core analysis by a two-step method. For instance, recently, the STREAM/RAST-K code system was verified and used for a two-step neutronic analysis of large-scale reactors, APR-1400 and OPR-1000 [25], and optimization of a new design of a small modular reactor SMPWR [26]. Following a similar approach, the PARCS/Serpent code system was used to model small-scale research reactors, including DNRR [27] and VR-1 [28].

However, in this study, the conventional CASMO-4/SIMULATE-3 computer program package, developed by Studsvik Scandpower, Inc. is used for this purpose. A data

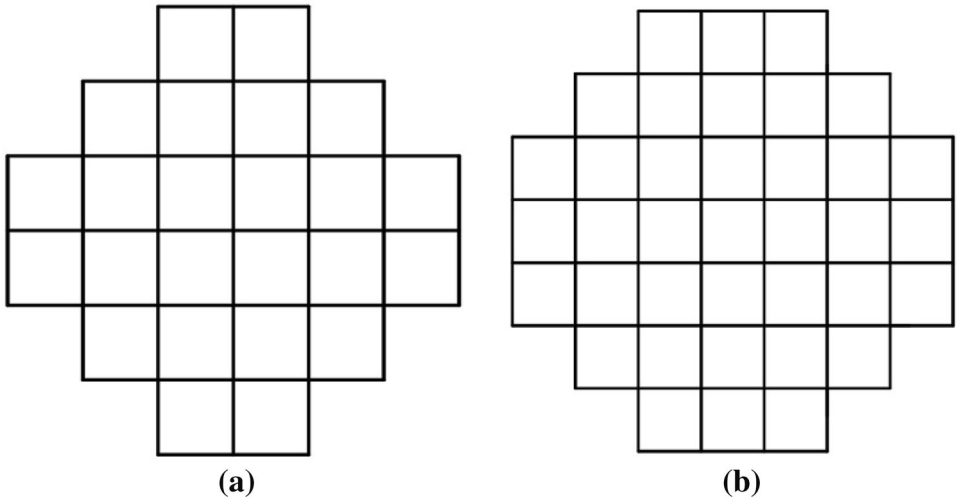

Fig. 2 Models: **a** Core A **b** Core B

Table 4 Core configurations parameters

Parameter	Core A	Core B
Thermal power (MW_{th})	150	150
Number of fuel assemblies	24	37
Number of fuel rods per assembly	236	236
Fuel rod height (cm)	150	100
Core equivalent diameter (cm)	114.8588	142.6132
Core volume (cm^3)	1.55×10^6	1.60×10^6
Fuel volume (cm^3)	4.48×10^5	4.60×10^5
Heavy metal mass (ton)	4.071	4.184
Power density (kW/L)	96.512	93.904
Linear power (W/cm)	176.5537	171.782
Specific power (MW_{th}/tonU)	36.84841	35.85251

library based on the evaluated data file ENDFIB-VI has been processed for lattice physics computations in CASMO-4. This library contains cross sections, decay constants, and fission yield for 337 materials. Then, CASMO-4, a multi-group, two-dimensional transport theory computer program for burnup calculations on fuel rods inside PWR assemblies, was used to obtain the averaged cross sections and neutron balances necessary for SIMULATE-3 [29]. The output was converted into a binary formatted nuclear data library by CMSLINK, a data processing program that links CASMO-4 to SIMULATE-3 [30]. For core calculation, SIMULATE-3, a three-dimensional advanced two-group nodal code based on the QPANDA neutronics model, was used to solve the diffusion equation for the neutron flux in each node [31]. Finally, using results obtained from CASMO-4/SIMULATE-3, core key physics parameters such as the power distribution, reactivity coefficients, and critical boron concentration were calculated.

2.6 Analysis

Using results obtained from CASMO-4/SIMULATE-3, the core key physics parameters such as:

- Multiplication factor
- Power distributions
- Reactivity coefficients
- Critical boron concentration
- Control rod worth
- Shutdown margin
- Minimum discharge burnup

were investigated to meet the design criteria and safety limits, where reactivity coefficients must be negative, shutdown margin is available, and control rod worth is capable of shutting down the reactor. Several iterations were done to find the best core configuration by making several improvements to achieve the optimum fuel loading pattern by changing the enrichment and burnable absorbers in the fuel. Furthermore, because this conceptual design is for a small-scale SMR, neutron leaks are expected, and the water radial reflector is inefficient. As a result, other reflector materials must be researched to find a better reflector for SMR. There are three advantages the reflector serves in this SMR. First, a reflected reactor does not need to be as large as an unreflected reactor to produce the same power amount. Second, in a reflected reactor, the peak to average power and the flux's shape are more flattened, and the flux curvature is usually lower. Finally, relative to an unreflected core, a reflected reactor needs less fuel to reach critical mass [32].

Even though the results in the next section are promising, there are various improvements that may be made if

the constraints in the CASMO-4/SIMULATE-3 codes are addressed. Because CASMO-4 is incapable of modeling other unique configurations of burnable poison, such as the centrally shielded burnable absorber (CSBA), only gadolinia and IFBA burnable poison types were investigated in fuel assemblies optimization. In addition, the effect of modifying the radial reflector thickness was not investigated in reflector optimization since SIMULATE-3 has a limitation in that the reflector thickness is fixed by default and cannot be changed.

3 Results and discussion

3.1 Fuel assemblies optimization

24 fuel assemblies in core A and 37 fuel assemblies in core B were optimized to flatten the power distribution and suppress excess reactivity while maintaining a long cycle length. For both models, 4.95% enrichment is used for fuel rods that do not contain burnable poison, while 2% enrichment is used for fuel rods that contain burnable poison. The optimization was primarily done by modifying the burnable poison content in burnable poison rods. To illustrate, more than 300 iterations of different loading patterns were tested, like the sample shown in Fig. 3. These loading patterns are made up of various APR-1400 fuel assembly types A0, B1, C2, and C3, each containing a different number of burnable poison rods of varying burnable poison weights between 8 w/o and 20 w/o.

Two types of burnable poison were tested, the Gadolinia mixed with the fuel (UO_2 – Gd_2O_3) and an IFBA (ZrB_2) coat occupying half of the fuel gap. Comparing the results of both types for the first loading pattern in Fig. 3, the Zirconium Diboride (ZrB_2) in IFBA had a weak effect in suppressing the reactivity. Therefore, the (B-10) loading should be increased significantly to decrease the high excess reactivity and power peaking factor, as shown in Table 5. Due to the high absorption cross section of (Gd-157) and the limitation in the CASMO-4 code in modelling other types/shapes of burnable poison, the Gadolinia was chosen as a burnable poison for both core A and core B.

The optimized loading patterns depicted in Fig. 4 are chosen based on an analysis of key physics parameters for all suggested loading patterns to meet the design criteria and safety margins. For example, excess reactivity was suppressed by achieving a multiplication factor of 1.13 close to the initial core value of APR-1400 and was achieved in both cores A and B. Burnable poison content was chosen to flatten the power distribution and achieving a power peaking factor of less than 1.8. In addition, negative reactivity coefficients at hot full power condition were calculated at three points, Beginning of Cycle (BOC), Middle of Cycle (MOC), and End of Cycle (EOC). The loading pattern of core A consists of three types of fuel assemblies, each with a different number of burnable poison rods and weight, while core B consist of four types of fuel assemblies, due to its width, as shown in Table 6. The fuel assembly A0, which contains no burnable poison, is loaded on the periphery. In contrast, the fuel assembly C3, which includes the highest content of burnable poison, is loaded in the center to flatten the power. The amount of fuel used in core A is 4.002749 MTU, while in core B it is about 4.102638 MTU.

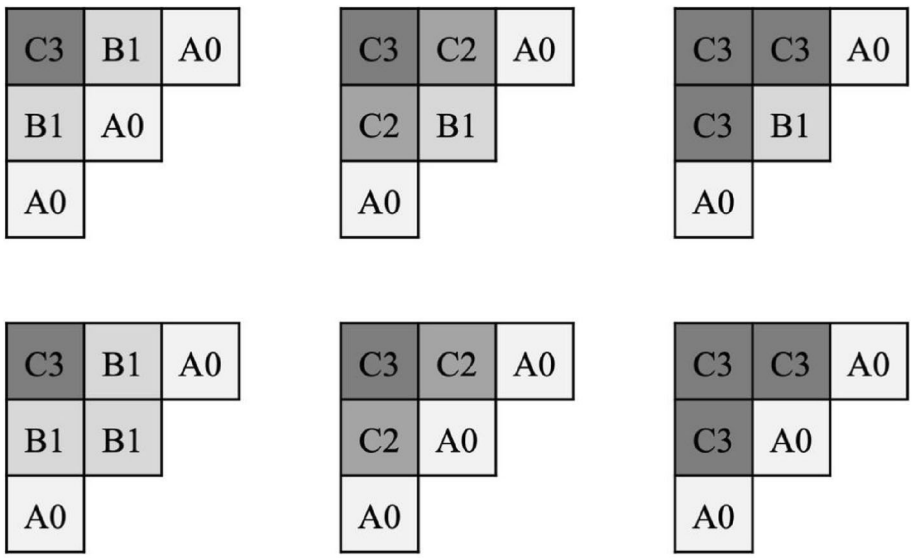

Fig. 3 Core A loading patterns sample

Table 5 Effectiveness of IFBA

B-10 Loading (mg/cm)	Excess reactivity (pcm)	$F_{xy} \times F_z$
0.772	19,345.73	2.33
2.316	17,569.28	2.22
10	13,156	1.93
20	10,777.22	1.77

3.2 Reflector optimization

Light water (H_2O) was initially used as the radial reflector for both core A and core B. Different radial reflector materials were proposed and tested to improve both models and reduce the expected high neutron leakage due to the small size of the SMR reactor. The material chosen for the reflector should have a low absorption cross section, a high scattering cross section, and a high density, all of which affect neutronic performance while also considering the material's thermal and mechanical stability at high temperatures and high radiation environments.

Tables 7 and 8 show the various materials proposed to replace the water radial reflector in cores A and B, respectively. Core A results are used for illustration purposes because the general behavior also applies to core B. Aside from the reduced total neutron leakage percentage of 13.6% of H_2O reflector in core A, several key physics parameters are calculated for comparison.

At first glance, the Magnesium Oxide (MgO) reflector appears to have superior power in reducing total neutron leakage to 10.9%. MgO has a high melting point at 2852 °C, and high moderating power due to the low atomic masses of Mg and O. However, the moderator temperature coefficient MTC of core A reflected by MgO at BOC is only −0.16 (pcm/°F), which is a marginal positive value results in instability and safety issues, makes it unsuitable.

When looking at the MTC as a measure for the best reflector material, the Tungsten Carbide (WC) reflector has the most negative MTC of −10.57 (pcm/°F), which is even better than the value of H_2O. However, WC is not selected as a reflector for this thermal reactor because it oxidizes at around 300 °C and has a minor cycle length enhancement. Beryllium (Be), Stainless Steel (SS), Beryllium Oxide (BeO), and Graphite (C) are the top four candidates for reflector material based on the MTC value.

The Be reflector is used in several research reactors due to its superior neutronic and material properties. Still, it is negatively affected by fast neutron irradiation, which causes reflector material degradation and swelling [33]. Moreover, given the high cost of the material, it is not economically feasible to use it as a long-term option.

Following that, Stainless Steel has power peaking factor, and moderator temperature coefficient MTC values similar to Be's. Analyzing the core A physics parameters shows better performance in terms of longer cycle length, lower peaking factor, and flat power distribution because the first peak has been moved to the second ring rather than the

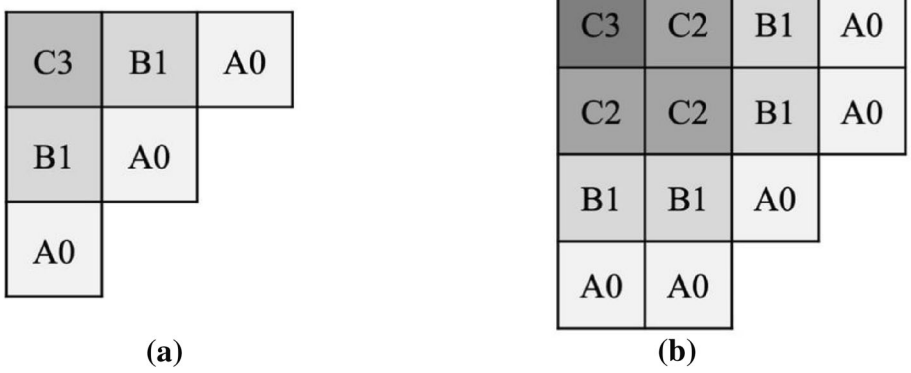

Fig. 4 Optimized loading patterns **a** Core A **b** Core B

Table 6 Loading patterns fuel assemblies

Assembly type	Enrichment (w/o)	#No. of Gd_2O_3 rods per assembly		Gd_2O_3 content (w/o)	
		Core A	Core B	Core A	Core B
A0	4.95	–	–	–	–
B1	4.95/2.00	12	12	8	8
C2	4.95/2.00	Not used	16	Not used	12
C3	4.95/2.00	16	16	18	18

Table 7 Reflector analysis of core A

Material	Total neutron leakage (%)	Peak ring	MTC at BOC (pcm/°F)	CBC (ppm)	$F_{xy} \times F_z$	2-batch B_d (GWd/MTU)	Cycle length (yr)
H_2O	13.60	1	−10.18	1753	1.78	32.58	1.19
Be	11.90	2	−5.81	2103	1.56	38.32	1.40
BeO	11.40	2	−4.25	2184	1.54	39.48	1.44
Graphite	11.30	2	−4.03	2192	1.54	39.41	1.44
MgO	10.90	2	−0.16	2254	1.53	40.17	1.46
SiC	11.10	2	−3.53	2219	1.54	39.70	1.45
SS	11.50	2	−5.36	2141	1.56	38.45	1.40
WC	12.90	1	−10.57	1892	1.70	34.49	1.26
Zr_3Si_2	11.10	2	−3.79	2210	1.54	39.52	1.44
ZrC	11.20	2	−3.93	2206	1.54	39.54	1.44
Zr	11.20	2	−3.96	2203	1.54	39.43	1.44
ZrO_2	11.10	2	−3.54	2223	1.54	39.77	1.45

Table 8 Reflector analysis of core B

Material	Total neutron leakage (%)	Peak ring	MTC at BOC (pcm/°F)	CBC (ppm)	$F_{xy} \times F_z$	2-batch B_d (GWd/MTU)	Cycle length (yr)
H_2O	12.80	1	−9.35	1758	1.59	38.42	1.43
Be	11.60	3	−7.27	1998	1.50	42.08	1.57
BeO	11.60	3	−6.19	2058	1.48	42.89	1.60
Graphite	11.50	3	−6.08	2062	1.48	42.82	1.60
MgO	11.20	3	−2.79	2107	1.47	43.36	1.62
SiC	11.40	3	−5.74	2080	1.48	43.01	1.61
SS	11.60	3	−6.93	2028	1.50	42.25	1.58
WC	12.40	3	−10.38	1848	1.56	39.70	1.48
Zr_3Si_2	11.40	3	−5.92	2073	1.48	42.95	1.60
ZrC	11.40	3	−5.99	2073	1.48	42.67	1.59
Zr	11.40	3	−6.03	2068	1.48	42.88	1.60
ZrO_2	11.30	3	−5.73	2086	1.48	43.07	1.61

center. While Stainless Steel is already used in the structural material of the core and the core baffle, its high strength ensures that it can withstand the harsh environment of the core.

BeO and Graphite can compete with Stainless Steel, but their MTC values are less negative. Silicon Carbide (SiC), Zirconium (Zr), and Zirconium compositions (Zr_3Si_2, ZrC, and ZrO_2) are also effective at reducing total neutron leakage. Still, their drawbacks stem from their less negative MTC due to the requirement of high critical boron concentrations, such as more than 2200 ppm in core A.

After comparing Stainless Steel to other suggested materials in core A and core B, it is concluded that Stainless Steel is the most suitable potential candidate for replacing the water radial reflector.

3.3 Best core configuration

The optimized core A and core B results with water and Stainless Steel reflectors are shown in Table 9. For this desalination SMR, it is recommended to select a radially larger and axially shorter core B model, shown in Fig. 5 with fuel assemblies in Table 10, reflected by Stainless Steel. This selection is based on an analysis of the following key physics parameters to meet the design criteria and safety margins.

Table 9 Summary of results

Model	Total neutron leakage (%)	ρ_{ex} (pcm)	F_{xy}	F_z	$F_{xy} \times F_z$	MTC at BOC (pcm/°F)	CBC at BOC (ppm)	B_d (2-batch) (GWd/MTU)	Cycle length (yr)
Core A (H_2O RR)	13.60	11,814.25	1.283	1.388	1.78	−10.18	1753	32.58	1.19
Core A (SS RR)	11.50	13,894.8	1.132	1.382	1.56	−5.36	2141	38.45	1.40
Core B (H_2O RR)	12.80	12,132.71	1.229	1.298	1.59	−9.35	1758	38.41	1.43
Core B (SS RR)	11.60	13,650.18	1.161	1.295	1.50	−6.93	2028	42.25	1.58

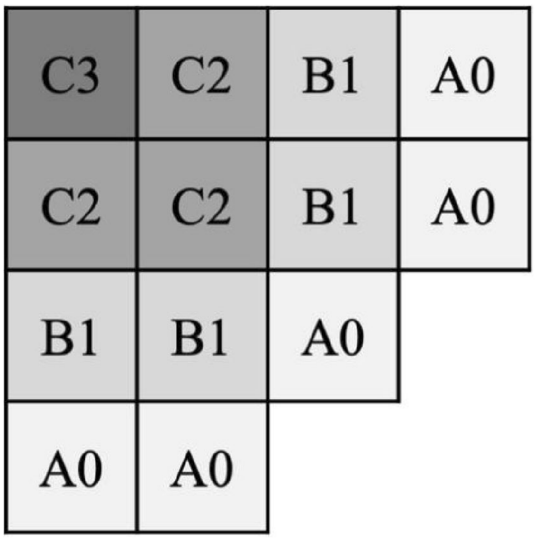

Fig. 5 Core B (SS RR) loading pattern

3.3.1 Multiplication factor

Figure 6 shows the multiplication factor as a function of burnup. This plot provides detailed information, such as the initial k_{eff} is 1.15808 implying that with the Stainless Steel reflector, the total neutron leakage was reduced to 11.6% and an initial excess reactivity of 13,650.18 pcm was saved, assuming Xe and Sm equilibrium. This core's single-batch reload plan will discharge the fuel at a burnup of 27.5 GWd/MTU every nearly two years.

3.3.2 Power distributions

Figure 7a and b depicts the radial and axial power distributions, respectively. The combined effect of this loading pattern, which used three different weights of burnable poisons, and the Stainless Steel reflector, has flattened the power distribution. Thus, the maximum radial power was reduced to 1.161 and the total power peaking factor to 1.50.

3.3.3 Reactivity coefficients

To comprehend the reactivity behavior in response to a change in one of the reactor parameters, the reactivity coefficients at hot full power conditions were calculated at three points: BOC (BU = 0 GWd/MTU), MOC (BU = 13.75 GWd/MTU), and EOC (BU = 27.5 GWd/MTU), as shown in Table 11. Overall, all reactivity coefficients had a desired negative value, highlighting the most important here, the moderator temperature coefficient (MTC) and the uniform doppler coefficient (UDP) representing the fuel temperature coefficient (FTC), where the reactivity decreases when the temperature increases. The MTC is −6.93 (pcm/°F), which is acceptable and can be made more negative by adapting a low/free soluble boron core, accomplished by implementing new burnable poison configurations. On the other hand, the boron does not affect the FTC, which is dominated by the effect of absorption in the resonances (Doppler broadening).

Table 10 Core B (SS RR) fuel assemblies

Assembly type	Enrichment (w/o)	#No. of Gd_2O_3 rods per assembly	Gd_2O_3 content (w/o)
A0	4.95	–	–
B1	4.95/2.00	12	8
C2	4.95/2.00	16	12
C3	4.95/2.00	16	18

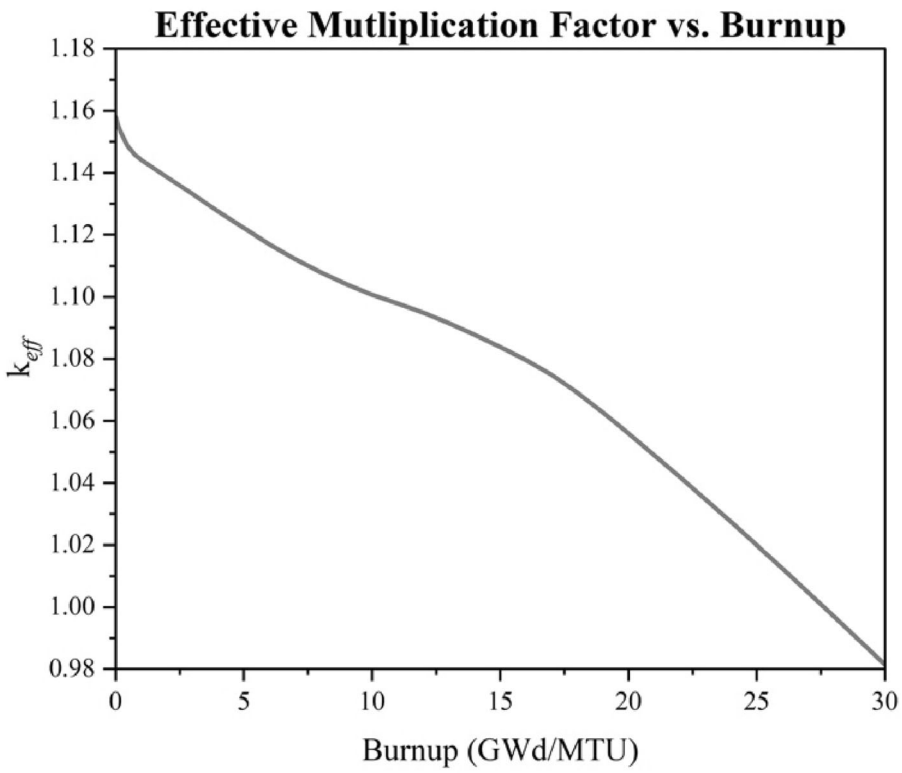

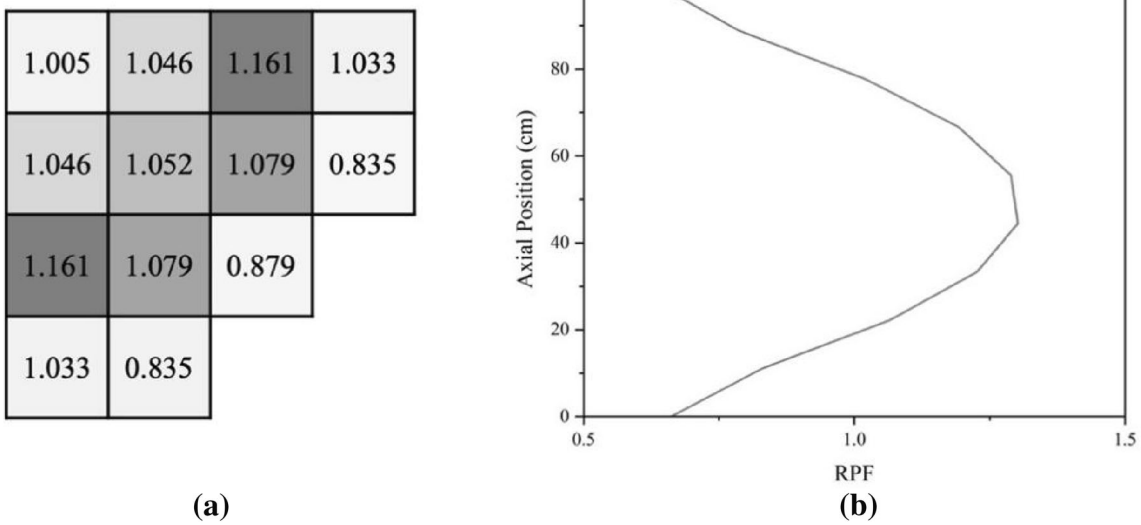

Fig. 6 k_{eff} vs. burnup of core B (SS RR)

Fig. 7 Power distributions of core B (SS RR): **a** Radially **b** Axially

3.3.4 Critical boron concentration

Excess reactivity can be reduced using two methods: the slow mechanism of injecting boron into the coolant or the fast mechanism of inserting the control rods. The boron concentration required to maintain criticality is plotted against the burnup in Fig. 8. To maintain the criticality of this model, the BOC must have a soluble boron concentration of 2028 ppm, while the EOC is indicated by a concentration of 16 ppm. Thus, in Table 11, the boron concentration effect on the moderator temperature coefficient has an acceptable negative value for reactor safety.

Table 11 Reactivity coefficients of optimized core B (SS RR) at (HFP)

Hot Full Power			
Coefficient	BOC	MOC	EOC
Isothermal Temperature Coefficient (ITC) (pcm/°F)	−8.34	−18.32	−32.9
Moderator Temperature Coefficient (MTC) (pcm/°F)	−6.93	−16.78	−31.21
Uniform Doppler Coefficient (UDP) (pcm/°F)	−1.41	−1.54	−1.7
Boron Coefficient (BOR) (pcm/ppm)	−6.34	−7.18	−10.64
Power Coefficient (POW) (pcm/Δpower%)	−0.71	−1.61	−2.96

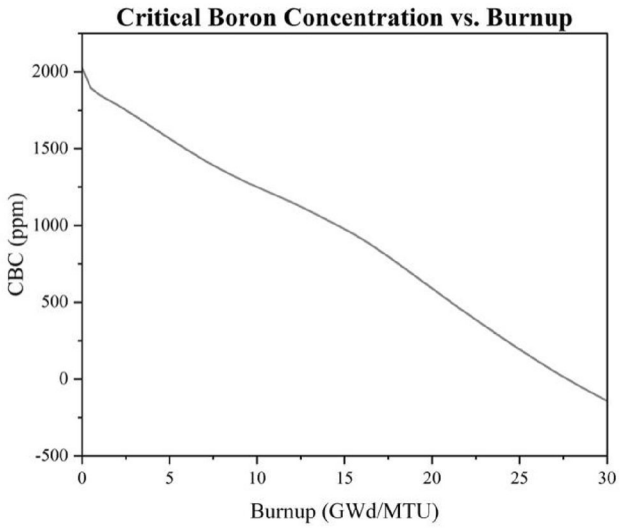

Fig. 8 CBC vs. burnup of optimized core B (SS RR)

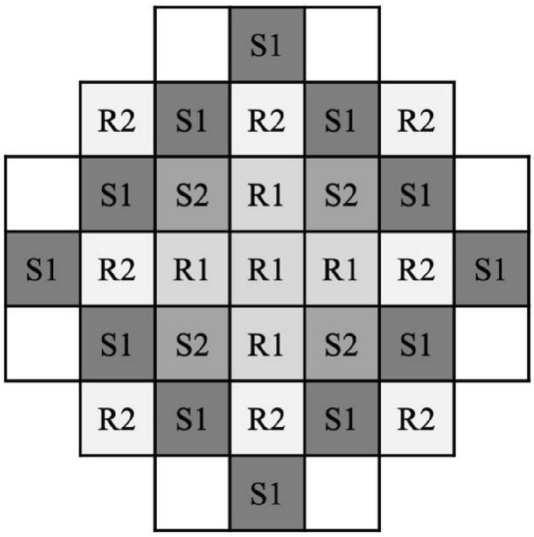

Fig. 9 Core B (SS RR) control banks pattern (R: Regulating, S: Shutdown)

3.3.5 *Control rod worth*

Control rods are used for quick control of reactivity during power maneuvering, shutdown, and scram. In this model, control rods in two regulating banks and two shutdown banks were tested. Figure 9 depicts the optimized control banks pattern, including one 12-finger regulating bank in the center, and the rest are of 4-finger banks. Figure 10a and b shows the detailed integral and differential worths of the four banks. The first regulating bank, as listed, has a total worth of 868.5 pcm, while the second has a total worth of 8622.2 pcm. For the first shutdown bank, the most substantial bank with a total worth of 10,793.3 pcm is chosen. Another shutdown bank with a total worth of 4117.7 pcm exists for redundancy. As can be seen, most differential values worths have some skewness; this may be because this is a short reactor with vast temperature differences between the inlet and outlet; as a result, neutron absorption is affected.

3.3.6 *Shutdown margin*

We must ensure that the reactor can be shut down when all control rods are inserted using the chosen control bank scheme. The shutdown margin is typically calculated by adding the total worth of all control rods and subtracting the excess reactivity while assuming the most reactive control rod is stuck. However, due to the shadowing effect, this approach cannot be used in this SMR model. Because it is a small core, it is susceptible to changes in position so that the result can be overestimated. Instead, a different approach was used here, which involved comparing the reactivity values when all control rods were withdrawn versus when all control rods were inserted. As shown in Table 12, at cold zero power condition (CZP), the insertion of all control rods with the presence of chemical shim will result in a negative reactivity of 8412.83 pcm. Thus, along with other negative reactivity contributions such as the burnable poison, it gives us confidence that we can shut down the reactor.

3.3.7 *Minimum discharge burnup*

To calculate the minimum discharge burnup, a quadratic reactivity model [34] has been used. As shown in Fig. 11, the reactivity is plotted as a function of the burnup and fitted by second order polynomial equation.

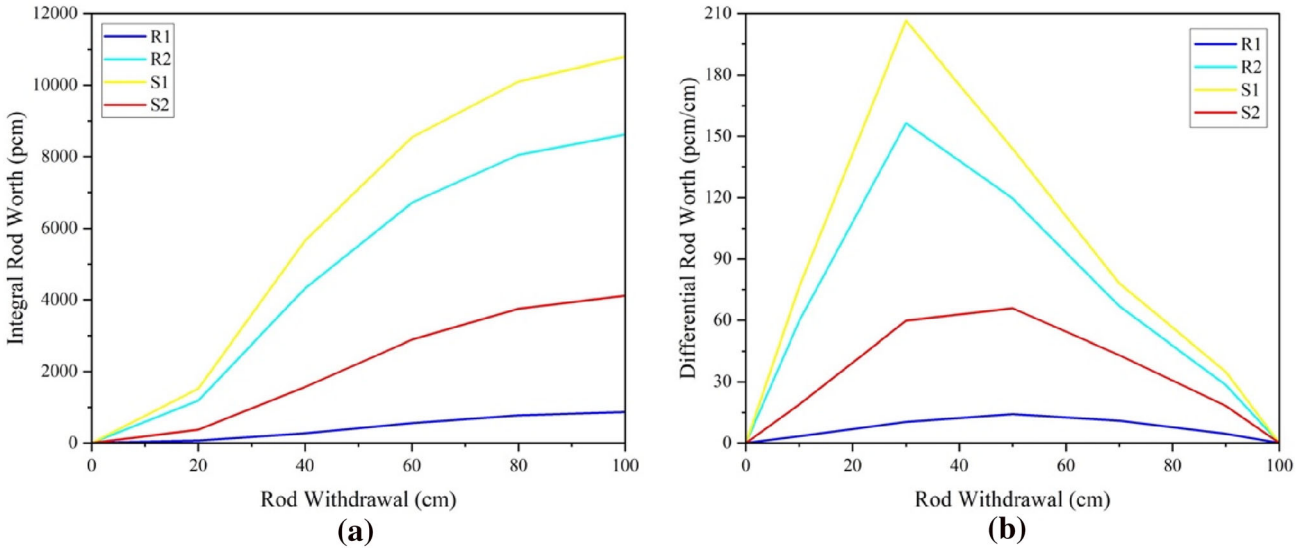

Fig. 10 Control banks worths: **a** Integral **b** Differential

Table 12 Control rods of core B (SS RR) conditions and reactivity

Condition	k_{eff}	ρ (pcm)
All Control Rods Out (0 ppm)	1.27806	21,756.41
All Control Rods In (0 ppm)	1.10239	9288.00
All Control Rods Out (1753 ppm)	1.03128	3033.12
All Control Rods In (1753 ppm)	0.9224	−8412.83
Control Rod Worth	−12,468.41 pcm	
Chemical Shim Worth	−18,723.28 pcm	

Table 13 Number of batches and their average cycle and discharge burnups of core B (SS RR)

n	B_c (GWd/MTU)	B_d (GWd/MTU)
1	27.5	27.5
2	21.13	42.25
3	17.18	51.54
4	14.56	58.24

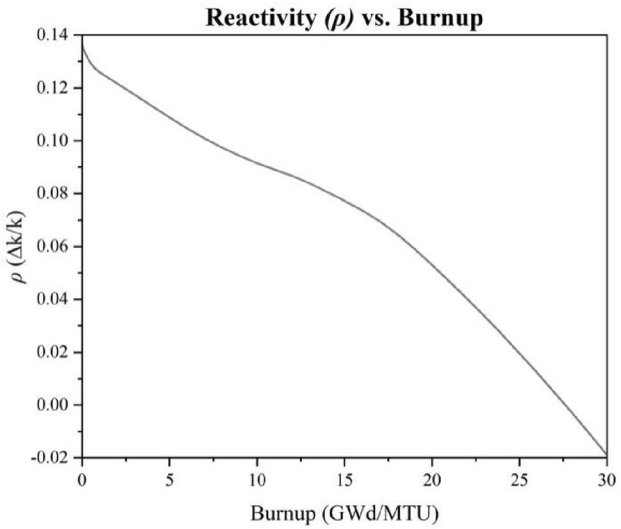

Fig. 11 Reactivity vs. burnup of core B (SS RR)

Table 13 lists the average cycle burnup and discharge burnup for reloading plans with up to four batches. As an option, a 2-batch reload plan corresponding to a 1.583-year cycle length is more favorable for this model because there is a significant difference while going from 27.5 GWd/MTU to 42.25 GWd/MTU. In contrast, the difference in burnups between 2-batches and 3-batches, as well as 3-batches and 4-batches, is much less. It is important to note that even with the lack of an accurate model to find the minimum discharge burnup with burnable poison in fuel, core B can achieve a higher burnup value than core A.

3.3.8 Comparison with other models

In Table 14, the general characteristics of core B with a Stainless Steel reflector are compared to the APR-1400 reference reactor and other SMR models. This SMR model has the highest specific power while using the smallest heavy metal mass discharged at the highest burnup value, compared with the SMART and NuScale models.

Table 14 Comparison with other SMR models [21] 24

Parameter	APR-1400	Core B (SS RR)	SMART	NuScale
Power (MWth)	3983	150	330	160
Core equivalent diameter (cm)	364.7	142.6	183.2	150.6
Active length (cm)	381	100	200	200
No. Fuel assemblies	241	37	57	37
Heavy metal mass (MTU)	103.82	4.1026	12.437	8.8
Specific power (kW/kgU)	38.36	36.56	26.54	18
Enrichment (max)	4.65%	4.95%	4.95%	4.95%
Reload plan (batches)	3	2	1	3
B_d (GWd/MTU)	28.91	42.25	36.1	> 30
Cycle length (yr)	1.5	1.58	3	2

4 Conclusion

This work investigated two conceptual 150 MW_{th} SMR core designs capable of supplying power up to 5 plants similar to the Ghalilah desalination plant, with a capacity of 68,000 m^3/d of desalinated seawater by reverse osmosis. Both cores A and B use the standard APR-1400 fuel assembly configuration, with some enrichment and burnable absorber modifications. The core models examine two-dimension parameters, with core A being radially smaller and axially taller and core B being radially larger and axially shorter. As a final decision, the core B model reflected by Stainless Steel was selected for this desalination SMR. This best configuration has a total neutron leakage of 11.60% and a reduced power peaking factor of 1.50. In addition, it met both the design and safety criteria by having negative reactivity coefficients and a sufficient shutdown margin. The chosen model will run for a 1.58-year 2-batch cycle until the fuel is discharged at a burnup of 42.25 GWd/MTU. Compared to the SMART and NuScale SMR models, this proposed design has the highest specific power while using the least heavy metal mass.

Future work aims to analyze the consistency of results and overcome the limitations encountered in CASMO-4 and SIMULATE-3 deterministic codes, both models can be tested using other computer codes based on the Monte Carlo approach. Additionally, a thermal–hydraulic analysis of the SMR core can be performed to ensure that it can be operated at steady-state and transient conditions without violating design parameters. Furthermore, by loading different types of burnable poison, an adaptation of a soluble boron-free core can be investigated to improve the MTC value. Finally, the desalination efficiency of this SMR can be increased by adopting a hybrid of thermal/electrical desalination processes and investigating the coupled system's corresponding thermodynamic cycle and economics.

Acknowledgements The authors would like to thank Dr. Victor Gillette for his constructive feedback. This research was supported by the Office of Vice Chancellor for Research & Graduate Studies, University of Sharjah, under grant no. V.C.R.G./R.1325/2021.

References

1. R. Chowdhury, M.M. Mohamed, A. Murad, Variability of extreme hydro-climate parameters in the north-eastern region of United Arab Emirates. Proc. Eng. **154**, 639–644 (2016). https://doi.org/10.1016/j.proeng.2016.07.563
2. M.S. Mohsen, B. Akash, A.A. Abdo et al., Energy options for water desalination in UAE. Proc. Comput. Sci. **83**, 895–896 (2016). https://doi.org/10.1016/j.procs.2016.04.181
3. V. Belessiotis, E. Delyannis, The history of renewable energies for water desalination. Desalination **128**(2), 157–158 (2000). https://doi.org/10.1016/S0011-9164(00)00030-8
4. H.T. El-Dessouky, H.M. Ettouney, *Fundamentals of Salt Water Desalination*, 1st edn. (Elsevier Science B.V, Amsterdam, 2002), pp.11–14
5. G. Alonso, E. del Valle, J.R. Ramirez, *Desalination in Nuclear Power Plants*, 1st edn. (Elsevier, United Kingdom, 2020), pp.23–44
6. G. Wetterau, S. Sethi, *Desalination of Seawater*, 1st edn. (American Water Works Association, United States, 2011), pp.3–28
7. J. Kucera, *Desalination: Water from Water*, 2nd edn. (Scrivener Publishing, Massachusetts, 2014), pp.18–23
8. N. Voutchkov, *Desalination Engineering Planning and Design*, 1st edn. (McGraw-Hill Companies, United States, 2013), pp.43–44
9. A. Al-Othman, N.N. Darwish, M. Qasim et al., Nuclear desalination: a state-of-the-art review. Desalination **457**, 43 (2019). https://doi.org/10.1016/j.desal.2019.01.002
10. International Atomic Energy Agency, Climate Change And Nuclear Power 2018. (IAEA, 2018), https://www.iaea.org/publications/13395/. Accessed 20 May 2022
11. The United Arab Emirates' Government Portal. UAE Energy Strategy 2050, https://u.ae/en/about-the-uae/strategies-initiatives-and-awards/federal-governments-strategies-and-plans/uae-energy-strategy-2050. 2021. Accessed 15 Nov 2021
12. The United Arab Emirates' Government Portal. The UAE Water Security Strategy 2036, https://u.ae/en/about-the-uae/strategies-initiatives-and-awards/federal-governments-strategies-and-plans/the-uae-water-security-strategy-2036. 2021. Accessed 15 Nov 2021
13. M.M. Megahed, Nuclear desalination: history and prospects. Desalination **135**, 177–181 (2001). https://doi.org/10.1016/S0011-9164(01)00148-5

14. International Atomic Energy Agency, Status of Nuclear Desalination in IAEA Member States. (IAEA, 2007), https://www.iaea.org/publications/7584/. Accessed 10 Oct 2021
15. Y. Shiota, Experience with Nuclear Desalination in Japan. (IAEA, 1996), https://inis.iaea.org/search/search.aspx?orig_q=RN:28009150. Accessed 10 Oct 2021
16. D.T. Ingersoll, Z.J. Houghton, R. Bromm et al., NuScale small modular reactor for co-generation of electricity and water. Desalination **340**, 86 (2014). https://doi.org/10.1016/j.desal.2014.02.023
17. S.H. Ghazaie, K. Sadeghi, E. Sokolova et al., Comparative analysis of hybrid desalination technologies powered by SMR. Energies **13**(19), 5006 (2020). https://doi.org/10.3390/en13195006
18. Y.P. Zhang, Y.W. Ma, J.H. Wu et al., Preliminary analysis of fuel cycle performance for a small modular heavy water-moderated thorium molten salt reactor. Nucl. Sci. Tech. **31**, 108 (2020). https://doi.org/10.1007/s41365-020-00823-5
19. L. Carlson, J. Miller, Z. Wu, Implications of HALEU fuel on the design of SMRs and micro-reactors. Nucl. Eng. Des. **389**, 111648 (2022). https://doi.org/10.1016/j.nucengdes.2022.111648
20. M.V. Ramana, L.B. Hopkins, A. Glaser, Licensing small modular reactors. Energy **61**, 555 (2013). https://doi.org/10.1016/j.energy.2013.09.010
21. International Atomic Energy Agency, Advances in Small Modular Reactor Technology Developments. (IAEA, 2020), https://aris.iaea.org/Publications/SMR_Book_2020.pdf. Accessed 25 Sep 2021
22. Aquatech International. Aquatech's 15 MIGD Desalination Plant helps the United Arab Emirates Reduce Dependence on Groundwater, https://www.aquatech.com/project/aquatechs-15-migd-desalination-plant-helps-uae-reduce-groundwater-dependence/. 2015 [accessed 2 Feb 2021]
23. The Sustainabilist, The Art of Desalination. (Dubai Carbon, 2018), https://issuu.com/dccepublications/docs/digital_issue_10. Accessed 5 Feb 2021
24. KEPCO & KHNP, APR1400 Design Control Document Tier 2. (Korea Electric Power Corporation & Korea Hydro & Nuclear Power Co., Ltd, 2018), https://www.nrc.gov/docs/ML1822/ML18228A651.pdf. Accessed 23 Feb 2021
25. J. Choe, S. Choi, P. Zhang et al., Verification and validation of STREAM/RAST-K for PWR analysis. Nucl. Eng. Technol. **51**, 356–368 (2019). https://doi.org/10.1016/j.net.2018.10.004
26. J. Jang, J. Choe, S. Choi et al., Optimization of Control Rod Operation for Soluble-Boron Free SMPWR with Zircaloy Reflector, *Paper Presented at Korean Nuclear Society 2019 Spring Meeting* (Jeju, Korea, 23–24 May 2019)
27. V.P. Tran, K.C. Nguyen, D. Hartanto et al., Development of a PARCS/Serpent model for neutronics analysis of the dalat nuclear research reactor. Nucl. Sci. Tech. **32**, 15 (2021). https://doi.org/10.1007/s41365-021-00855-5
28. F. Fejt, P. Suk, J. Frybort et al., Utilization of PARCS/Serpent in small-scale reactor—multiplication factor, rod worth, and transient. Ann. Nucl. Energy. **166**, 108757 (2022). https://doi.org/10.1016/j.anucene.2021.108757
29. S. Scandpower, *CASMO-4 A Fuel Assembly Burnup Program User's Manual, SSP-09/443-U Rev 0* (Studsvik Scandpower Inc., United States, 2009)
30. S. Scandpower, *CMS-LINK User's Manual, SSP-09/444-U Rev 0* (Studsvik Scandpower Inc., United States, 2009)
31. S. Scandpower, *SIMULATE-3 Advanced Three-Dimensional Two-Group Reactor Analysis Code, SSP-09/447-U Rev 0* (Studsvik Scandpower Inc., United States, 2009)
32. J.R. Lamarsh, A.J. Barratta, *Introduction to Nuclear Engineering*, 3rd edn. (Pearson Education Limited, England, 2014), pp.296–304
33. P.S. Bejarano, R.G. Cocco, Beryllium Reflectors for Research Reactors, *Paper Presented at 4th International Symposium on Material Testing Reactors Conference* (Oarai, Japan 5–9 Dec. 2011)
34. G.T. Parks, J.D. Lewins, Quadratic reactivity fuel-cycle model. Ann. Nucl. Energy. **14**(3), 145–151 (1987). https://doi.org/10.1016/0306-4549(87)90088-0